Estimating the carbon content of the deep mantle with Icelandic melt inclusions

William G.R. Miller[a,*], John Maclennan[a], Oliver Shorttle[a,b], Glenn A. Gaetani[c], Véronique Le Roux[c], Frieder Klein[c]

[a] *Department of Earth Sciences, University of Cambridge, Downing Street, Cambridge, CB2 3EQ, UK.*
[b] *Institute of Astronomy, University of Cambridge, Madingley Road, CB3 0HA, UK.*
[c] *Woods Hole Oceanographic Institution, Woods Hole, MA 02543, USA.*

Abstract

Earth's carbon budget is central to our understanding of the long-term co-evolution of life and the planet. Direct observations of surface reservoirs allow for the detailed quantification of their carbon content. However, the carbon content of Earth's deep interior remains poorly constrained. Here we study olivine-hosted melt inclusions from two Icelandic eruptions, with those from the Miðfell eruption allowing us to investigate the carbon content of the deep mantle. Comparison with the previously studied Borgarhraun eruption highlights the presence of deep, plume-sourced mantle material within the Miðfell source region. Miðfell contains trace element-depleted melt inclusions undersaturated in CO_2, which have high CO_2/Ba (= 396 ± 48) and CO_2/Nb (= 1832 ± 316), though some inclusions preserve even greater relative carbon enrichment. These observations allow us to reconstruct the CO_2 content of the bulk Miðfell source as being > 690 ppm. By identifying that Miðfell is a mixture of depleted and deep mantle components, we can estimate a CO_2 content for the deep mantle component of 1350 ± 350 ppm; a concentration that is over ten times higher than depleted MORB mantle estimates. Assuming that the deep mantle component

*corresponding author: wm248@cam.ac.uk

identified in Miðfell is representative of a global reservoir, then with our new CO_2 estimate and by considering a range of representative mantle fractions for this reservoir, we calculate that it contains up to 14 times more carbon than that of the atmosphere, oceans, and crust combined. Our result of elevated CO_2/Ba and CO_2/Nb ratios, and carbon enrichment support geochemical bulk Earth carbon models that call for the presence of carbon-rich deep mantle domains to balance Earth's relatively carbon-poor upper mantle and surface environment.
Keywords: Deep mantle carbon; Iceland, melt inclusions

1. Introduction

Geological processes have modulated the Earth's atmospheric carbon content for billions of years (Hayes and Waldbauer, 2006). At the heart of this cycle is a partitioning of carbon between planetary reservoirs, one that has placed the overwhelming majority of carbon in Earth's crust, mantle, and core (e.g., Dasgupta and Hirschmann, 2010). The carbon flux from these solid-Earth reservoirs to the atmosphere is efficiently returned via silicate weathering (e.g., Walker et al., 1981), maintaining a habitable climate, and closing the loop on a cycle that has helped maintain liquid water at Earth's surface over almost its entire history (Mojzsis et al., 2001).

To understand how Earth has come to operate such a stable and long-lasting chemical cycle, it is key to know how carbon is distributed among its reservoirs (Hirschmann, 2016). Whilst for the atmosphere, oceans, and to some extent the crust, their carbon content can be measured directly, quantifying the carbon content of mantle reservoirs is more challenging. Two basic problems frustrate accurate estimation of mantle carbon content: (i) the low solubility of carbon in basaltic melts (Shishkina et al., 2010), which means that information on high-carbon mantle domains is preferentially lost as their melts begin to degas at high pressure in the crust or shallow mantle; and (ii) the partial view that

volcanism provides of the mantle, with the vast majority of magmas tapping the depleted upper mantle. Only rarely do volcanics display evidence for the involvement of deep-sourced material in their petrogenesis: such occurrences are usually linked to the presence of mantle plumes. These compounding problems cause considerable uncertainty in previously published mantle carbon estimates.

In this paper we present new observations that help constrain the amount of carbon in the deep mantle reservoir. In Section 2, we review the geochemical constraints available on mantle carbon, and identify the observational gaps in our present reservoir inventories. We next present our methods (Section 3) and new data (Section 4) from two Icelandic eruptions, demonstrating that their geochemical characteristics are suited to quantify the amount of carbon in the deep mantle. We show that one of these eruptions, Miðfell, contains melt inclusions that are undegassed and relatively enriched in carbon compared to lithophile trace elements of similar mineral-melt compatibility (Section 5). In Section 6, we use these results to place a new constraint on the deep mantle carbon content, and in Section 7 discuss the implications of this constraint for the origin and distribution of carbon in the Earth.

2. Measuring mantle carbon

An enormous amount of work, especially over the last two decades, has focused on measuring the carbon content of mantle-derived volcanics. Despite this effort, surprisingly few observations provide tight constraints on upper mantle carbon content, and fewer still on deep mantle carbon. This section aims to contextualise the present study with this body of work, and identify the features that, in subsequent sections, will mark our new observations as distinct from pre-existing data sets.

2.1. The upper mantle

Mid-ocean ridge basalts (MORBs) sample the most accessible mantle reservoir, the depleted MORB mantle (DMM). Although a shallow reservoir in the context of the mantle, the DMM can be a component of deep-sourced mantle plume magmas, as is the case on Iceland (Stracke, 2012).

A key technique for estimating carbon in DMM is to find an incompatible lithophile trace element (ITE) to reference MORB carbon concentrations against, thereby providing a control for fractionation during mantle melting and crustal differentiation. Estimates of source mantle ITE concentration (e.g., Workman and Hart, 2005) then enable calculation of a source carbon content. Ba and Nb are commonly chosen as reference elements because they have similar compatibility to carbon during peridotite melting (Rosenthal et al., 2015). However, as Ba and Nb are not volatile, accurate estimation of source carbon is dependent on either finding melts that are CO_2 undersaturated, or reconstructing pre-degassed CO_2. A degassing correction has been applied to some highly vesicular glass samples, which re-coupled CO_2 to ITE concentrations, giving DMM carbon estimates of 393 $\pm$ 82 ppm CO_2 using CO_2/Nb = 534, and 427 $\pm$ 45 ppm CO_2 using CO_2/Ba = 106 (Table 1; 14°N Mid-Atlantic Ridge; Cartigny et al., 2008). We note that whilst carbon exists in the mantle in oxidised and reduced forms (Dasgupta and Hirschmann, 2010), for ease of comparison between data sets, we report total carbon as CO_2.

Only rare suites, such as some pillow glasses erupted at relatively high pressure and with intrinsically low carbon content, may show undersaturated volatile concentrations. Michael and Graham (2015) used such samples to estimate a DMM CO_2 of 59 $\pm$ 39 ppm (Table 1; CO_2/Ba = 105; Global MORB). A difficulty with this approach is in having confidence that measured melts are truly undegassed. Saal et al. (2002) emphasised how linearly correlated carbon-trace

element concentrations can validate a data set as having undersaturated melt populations. However, Matthews et al. (2017) presented a forward model to suggest that such correlations can readily arise from the mixing of variably degassed melts at low pressure. They concluded that to have more confidence in identifying undegassed melts, data will ideally show some melts with high ITE content that have clearly degassed to their saturation concentration (i.e., no ITE-carbon correlation), and others with lower ITE and carbon content where an ITE-carbon correlation persists; such suites evidence incomplete melt mixing. Data sets exhibiting such structure offer the best chance for empirically separating degassed and undegassed melt populations.

Applying the insights from Matthews et al. (2017) can make certain data sets difficult to empirically validate for carbon undersaturation. For example, observations of quenched matrix glasses, for which the melt has been largely homogenised prior to eruption (i.e., many seafloor basalts; Shorttle, 2015; Michael and Graham, 2015), do not provide data sets that can be internally validated: giving only one CO_2 and ITE content per eruption. One solution is to use olivine-hosted melt inclusions, which, when trapped at high pressure, may capture melts with both undegassed carbon and chemical diversity that has not been homogenised by mixing (Maclennan, 2008b). Melt inclusion studies have thus been key in characterising upper mantle carbon: their results suggest that the DMM contains carbon heterogeneity, as both CO_2/ITE ratios and estimated ITE concentrations vary (Le Voyer et al., 2017), with carbon concentrations ranging from 22–427 ppm CO_2 (Table 1; Siqueiros, Saal et al., 2002; Mid-Atlantic Ridge, Cartigny et al., 2008, Le Voyer et al., 2017).

2.2. The deep mantle

We use the term 'deep mantle' to refer loosely to the region of Earth's convecting mantle that is not represented by the composition of typical MORB.

The geometry of this reservoir is poorly constrained, and its upper horizon could fall anywhere from the mantle transition zone, to the large low shear velocity provinces above the core-mantle boundary (e.g., Hofmann, 1997). Upwelling plumes can bring this deep mantle material into the upper mantle and melt it at shallow levels. Whatever its locus, the deep mantle appears to comprise primitive material that has remained isolated for billions of years (e.g., Mukhopadhyay, 2012; Peters et al., 2018), as well as crustal material introduced via recycling processes (e.g., Nestola et al., 2018). Both components could be significant carbon reservoirs: primitive material potentially containing solar nebular carbon, which dissolved into Earth's early magma ocean along with noble gases (e.g., Williams and Mukhopadhyay, 2018); whereas, recycled material could introduce organic or inorganic carbon from the surface (e.g., Nestola et al., 2018).

Ocean island basalts (OIBs) are prime candidates in the search for deep mantle carbon. Geochemical observations have consistently shown OIB to have more evidence of both recycled and primitive mantle components than MORB (e.g., Hofmann, 1997), and in many cases geophysical observations support their lower mantle origins (e.g., Montelli et al., 2006). Beneath Iceland specifically, the hot, low velocity, plume conduit has been seismically imaged through the deflected transition zone (Jenkins et al., 2016), and down into the lower mantle (Yuan and Romanowicz, 2017).

The nature of magma generation and eruption at ocean island settings typically results in OIB degassing (Gonnermann and Mukhopadhyay, 2007): low eruption or melt inclusion entrapment pressures combine with high initial dissolved CO_2 content, derived from low degree melting and/or carbon-rich source material. This degassing can, however, be an advantage if rather than measuring the melt, the degassed CO_2 flux is measured. Anderson and Poland (2017) mea-

sured CO_2 degassing at Hawaii, along with a melt production rate to estimate the Hawaiian source mantle carbon content to be 962 + 296/- 227 ppm CO_2. This estimate is significantly higher than that obtained from MORB (Table 1), a discrepancy suggesting the presence of high carbon regions in Earth's deep mantle. However, bulk degassing cannot be used to uniquely assign carbon to the recycled (e.g., Sobolev et al., 2005) or primitive (e.g., Trieloff et al., 2000) components inferred for the Hawaiian source. Our approach minimises this ambiguity by focusing on melt inclusions from single eruptions.

2.3. Bulk silicate Earth carbon estimates

In principle, the size of the bulk silicate Earth (BSE) carbon reservoir could be reconstructed using carbon estimates of all mantle reservoirs, including the deep mantle. However, as emphasised above, a key piece of information is poorly known: the size of this deep mantle reservoir (Hofmann, 1997). A common approach to this problem is to assume, or infer from geochemical mass balance, the size of the deep mantle reservoir and then use carbon-gas or carbon-trace element ratios to extrapolate to bulk Earth.

A recent review paper from Halliday (2013) presented several models for estimating bulk Earth carbon content. The 'basalt' model used the water content of MORB and OIB to infer a bulk water content for the entire mantle, and then took representative H/C ratios to calculate a bulk mantle carbon content (163 ppm CO_2). The 'layered mantle' model used Ar isotope budgets across all Earth's reservoirs, along with volatile ratios, to derive a bulk Earth carbon budget of 2462 ppm CO_2. This estimate is very similar to the value from Marty (2012), who also used an ^{40}Ar budget to extrapolate observed C/N and C/^{4}He ratios to the whole Earth (2831 ppm CO_2).

Carbon-ITE ratios in MORB, enriched-MORB, and OIB have also been used to reconstruct BSE carbon. Hirschmann (2018) presented a recent implementa-

tion of this approach, taking CO_2/Ba = 100 ± 20 for the convecting mantle and a representative Ba concentration to estimate 514 ± 147 ppm CO_2 in BSE. This new estimate assumes that oceanic basalts, regardless of enrichment, preserve similar CO_2/Ba ratios, and that analysed oceanic basalts sample all significant geochemical reservoirs within the Earth. Our new results will show, in contrast, that there is evidence for both significant CO_2/Ba variability, and that there exist mantle reservoirs with far higher CO_2/Ba than have previously been identified in MORB or OIB.

Whilst the above BSE carbon estimates vary significantly, they have a common implication: assuming DMM carbon concentrations of 20–100 ppm CO_2 (e.g., Dasgupta and Hirschmann, 2010), a significantly more carbon-rich reservoir must exist in the deep Earth to balance high BSE carbon estimates. For example, Hirschmann (2016) calculated that this reservoir needs CO_2/Nb = 5000 ± 2000 and CO_2/Ba = 850 ± 350 to match the BSE carbon content calculated by Marty (2012).

2.4. Carbon in the Icelandic mantle

Previous studies of Icelandic geothermal fluids, glasses and vesicles have concluded that the Icelandic mantle source has little to no carbon enrichment with respect to DMM. While these studies used bulk analyses to assess average source carbon, our study uses olivine-hosted melt inclusions to access signals of source heterogeneity that are preserved in melts prior to mixing.

Only one melt inclusion suite from Iceland has previously been interrogated for mantle carbon signatures; the Borgarhraun eruption in the Northern Rift Zone (NRZ, Fig. 1a). Olivine-hosted melt inclusions from Borgarhraun record compositional heterogeneity (Maclennan et al., 2003), show evidence of concurrent crystallisation and melt mixing (Maclennan, 2008a), and preserve a CO_2-ITE correlation (Hauri et al., 2018), which has been used as evidence for

an undegassed CO_2 signature (CO_2/Ba = 48.3 ± 2.7, CO_2/Nb = 391 ± 16; Table 1). The mantle carbon content inferred from these observations is similar to that of DMM, with CO_2/Nb comparable to undegassed MORB suites (Table 1), but with CO_2/Ba half the inferred global average (Hirschmann, 2018).

Borgarhraun melts are not strongly enriched in lithophile elements, being depleted relative to other Icelandic melts, and its He isotope signature (R/R_a = 7.9; Fig. 1b) lies within the MORB range (Füri et al., 2010). Hauri et al. (2018) suggested that the Borgarhraun mantle contains a source common to the Atlantic depleted mantle: hydrated and carbonated material originating from subduction-related modification. These features strongly suggest that there is no deep mantle component in the Borgarhraun source, which fits the regional systematics of 'MORB-like' He-Ne in NRZ eruptions in contrast to more 'solar-like' noble gas compositions of Western Rift Zone (WRZ) eruptions (e.g., Füri et al., 2010). Such observations align with Pb isotope constraints indicating distinct mantle source components across Iceland (Shorttle et al., 2013), and merit investigation of whether there are associated differences in mantle carbon abundances between the two rift zones. Our new observations from eruptions in the WRZ and central Iceland (Fig. 1a) directly address this question.

3. Samples and methods

3.1. Geological context

We present new data from two Icelandic eruptions, Miðfell (also known as Dagmálafell; 64° 10.456' N, 021° 02.859' W) and Kistufell (64° 47.442' N, 017° 10.456' W; Fig. 1a). Miðfell is a ∼300 m high mountain in Iceland's WRZ, lying on the eastern edge of Þingvallavatn and within the Hengill volcanic system. It is a northeast-southwest striking ridge, which is thought to have erupted beneath ice during the last glacial period (Gurenko and Chaussidon, 1995, and

references therein). The mountain's lower flanks comprise vesicular, olivine-phyric, pillow basalts with glassy rinds, whereas the upper portions are composed of hyaloclastite. Kistufell is a table mountain located in central Iceland, at the northern edge of Vatnajökull. Kistufell may have erupted towards the end of the last glacial period as the ice-sheet retreated (Breddam, 2002). Glassy pillows are exposed at the northern flanks of the mountain.

3.2. Geochemical context

Previous Miðfell melt inclusion studies have measured significant trace element variability, including high-degree melts with diluted ITE concentrations (Gurenko and Chaussidon, 1995). If carbon remained coupled to these ITE's, then it is likely that some Miðfell melt inclusions have avoided degassing, providing an opportunity to recover mantle carbon content. Both Miðfell and Kistufell have noble gas isotope data that support the presence of primordial material in their source regions: R/R_a ~17 (Breddam et al., 2000; Füri et al., 2010) and, where heavy noble gases have been measured in Miðfell, primordial Xe and Ne isotopic ratios (Mukhopadhyay, 2012). Miðfell olivines and matrix glass also show noble gas evidence for other components, including recycled air (e.g., Harrison et al., 1999). Combined, these observations make Miðfell and Kistufell good targets for identifying deep mantle carbon.

3.3. Analytical methods

Olivine phenocrysts 0.5–4 mm in size were picked from hand-crushed pillow glasses. Care was taken to pick unaltered olivine macrocrysts containing glassy melt inclusions without post-entrapment crystals. Olivines were individually mounted and polished to expose melt inclusions before being re-mounted and polished for analysis. Melt inclusions were analysed for trace elements, CO_2, and H_2O by secondary ion mass spectroscopy at the Edinburgh ion microprobe

facility. Major elements were measured by electron probe microanalysis. A subset of the Miðfell melt inclusion suite was processed at Woods Hole Oceanographic Institution to reconstruct their initial CO_2 content from vapour bubble and inclusion glass CO_2 concentrations. Melt inclusion and vapour bubble volumes were determined by X-ray tomography. Vapour bubble CO_2 content was determined using confocal Raman spectroscopy. For full method details and representative melt inclusion micrographs, see Supplementary Material.

4. Results

4.1. Major elements

Miðfell olivine phenocryst compositions range from $Fo_{90.9}$ to $Fo_{85.2}$ (Fig. 2), the matrix glass and olivine-hosted melt inclusion compositions are basaltic (SiO_2 ∼48 wt%), giving a picritic whole rock composition (Gurenko and Chaussidon, 1995). Kistufell olivines range from $Fo_{89.7}$ to $Fo_{87.9}$ with basaltic melt inclusions (SiO_2 ∼48 wt%).

Melt inclusion major element compositions have been corrected for post-entrapment crystallisation by iteratively adding an equilibrium olivine composition, assuming an Fe-Mg $K_D = 0.34$ (Matzen et al., 2011), until the melt inclusion reached equilibrium with its host (Danyushevsky et al., 2000). For Miðfell, this correction takes into account the ferric iron content of each melt inclusion (see Supplementary Material), whereas for Kistufell we assumed a constant ferric to total iron ratio of 0.07 based on matrix glass measurements (Breddam, 2002). The majority of melt inclusions required $< 5\%$ olivine addition to bring them back into Fe-Mg equilibrium with their olivine host.

4.2. Trace elements

Miðfell melt inclusions record substantially more variability than those from Kistufell (Fig. 2 & 3). The method of Maclennan et al. (2003) was used to

establish that the Miðfell analyses for all major, trace, and volatile elements (apart from H_2O, Yb and Lu) have a signal-to-noise ratio > 1, and $> 99\%$ confidence that natural variability can be resolved from analytical noise. These inclusions preserve trace element variability comparable with that found by the combination of all previously published undegassed melt inclusion and MORB glass suites (e.g., Saal et al., 2002). Kistufell melt inclusions recover a signal-to-noise ratio > 1 for the majority of major, trace, and volatile elements. However, the Kistufell melt inclusion suite has much lower melt heterogeneity than Miðfell, as indicated by their contrasting signal-to-noise ratios (e.g., Miðfell $\sigma_t/\sigma_r|_{Ba} = 86.4$; Kistufell $\sigma_t/\sigma_r|_{Ba} = 3.06$).

Multi-element plots (Fig. 3) illustrate Miðfell and Kistufell trace element variability compared to that of the Borgarhraun eruption (Hauri et al., 2018). As is typical for many mantle-derived basalts, the most incompatible trace elements show the largest concentration range. In Miðfell, Ba content ranges from 0.37–115 ppm (29.8–3.5% relative error; matrix glass 6.3 ppm), and Nb content ranges from 0.04–22.9 ppm (17.6–9.1% relative error; matrix glass 0.78 ppm). Vapour bubbles only occur in Miðfell melt inclusions with high trace element concentrations (> 12.4 ppm Ba and > 2.47 ppm Nb). Kistufell melt inclusions rarely contain vapour bubbles, so no inclusions with vapour bubbles were measured for this data set. Trace element patterns in all three eruptions show that some of the melt inclusions preserve positive Sr and negative Zr anomalies, consistent with previous Miðfell melt inclusion analyses (Gurenko and Chaussidon, 1995).

4.3. Volatile elements

Kistufell melt inclusions have a water content that matches that of the matrix glass surrounding host olivines, but the sample population shows some variability (0.10–0.19 wt%). Water content in the Miðfell melt inclusions and matrix

glass is almost constant at ∼0.06 wt%, which is low compared to other Icelandic melt inclusion suites (e.g., Laki, ∼0.65 wt% H_2O, Hartley et al., 2015). Melt inclusion CO_2 content varies from 20–1120 ppm (Fig. 4a). At low trace element concentrations (Ba $<$ 3.0 ppm, Nb $<$ 0.2 ppm) the maximum melt inclusion CO_2 content is controlled by CO_2/ITE ratios. At higher trace element concentrations, maximum CO_2 content reaches a plateau at 1120 ppm. Melt inclusions containing vapour bubbles record a glass CO_2 content of 720–1170 ppm, consistent with the vapour bubble-absent inclusions, and a total (reconstructed) CO_2 content of 1340–4550 ppm (Fig. 4a). Matrix glass has a CO_2 content of $<$ 200 ppm.

4.4. CO_2/ITE ratios

Kistufell melt inclusions record maximum CO_2/Nb = 391 ± 70 and CO_2/Ba = 71.9 ± 13.9, which are associated with the lowest ITE concentration melts. Miðfell melt inclusions preserve maximum CO_2/Nb = 5737 ± 987 and CO_2/Ba = 566 ± 68, also associated with low trace element concentrations, i.e., lower than the matrix glass (Fig. 5), and hosted in the most forsterite-rich olivines (Fig. 2b). Melt inclusions with CO_2 content reconstructed from vapour bubble concentrations also have high CO_2/ITE ratios, with maximum CO_2/Nb = 1186 ± 127 and CO_2/Ba = 236 ± 25. Comparison to previously analysed melt inclusion and MORB glass suites shows that the Miðfell melt inclusions preserve some of the highest CO_2/ITE ratios ever measured in natural basaltic glass (e.g., Le Voyer et al., 2017). Importantly, Miðfell inclusions exhibit these higher CO_2/ITE ratios at the same ITE concentrations as in previously studied suites, indicating that their relative carbon enrichment is not a feature of anomalous trace element depletion or enrichment (Fig. 5).

5. Does Miðfell preserve a mantle carbon signature?

The previous section demonstrated that whilst Miðfell melt inclusions preserve significant trace element variability, Kistufell contains a more homogeneous melt inclusion population. On this basis, the Kistufell melt inclusions do not enable empirical validation of whether they have degassed carbon (Fig. 4b; Matthews et al., 2017). However, Kistufell melt inclusions have ITE concentrations that in the Miðfell melt inclusion population are associated with carbon loss (Fig. 4). For Miðfell, this carbon loss is shown by systematically decreasing CO_2/ITE ratios with increasing ITE concentration (Fig. 5c,d). Kistufell inclusions have likely degassed, therefore we focus our investigation of deep mantle carbon onto the Miðfell inclusions, where we can be sure of recovering undegassed systematics.

Trace element and CO_2 data from Miðfell melt inclusions suggest that some process has enriched these basaltic glasses in carbon, relative to ITE's, compared with other inclusion and glass suites (e.g., Michael and Graham, 2015). To use this observation to constrain the carbon content of the Miðfell mantle source first requires an assessment of the influence of crustal processes, which could have affected the carbon and ITE content of Miðfell melts.

5.1. Degassing and olivine decrepitation

The strongest signal in the Miðfell CO_2 data, seen most clearly at trace element concentrations greater than that of the matrix glass, is one of degassing (Fig. 4a). At these high ITE concentrations, melt inclusions with variable trace element concentrations have constant CO_2 content, indicating the partial loss of initial CO_2, and therefore loss of information on carbon from deeper in the system. If degassing occurred in some of the Miðfell melts prior to entrapment, then solubility models suggest entrapment pressures of $\sim$1.8 kbar (taking 1170 ppm CO_2; Shishkina et al., 2010).

However, the presence of vapour bubbles in some of the trace element enriched melt inclusions suggests that some Miðfell melts were initially trapped with higher dissolved CO_2 concentrations and underwent exsolution post-entrapment. Reconstructed CO_2 concentrations from these inclusions are consistent with saturation pressures of up to ∼4.5 kbar (∼13 km depth). If all melts started with the same CO_2/ITE ratio, then those CO_2-saturated melt inclusions lacking vapour bubbles must have lost exsolved CO_2 during ascent to eruption, perhaps by decrepitation (Maclennan, 2017).

ITE-rich Miðfell melts appear to have been degassed to their saturation concentration, but at lower ITE concentrations melts show an ITE-CO_2 correlation. This observation suggests that ITE-depleted melt inclusions preserve an undegassed CO_2 signal (Matthews et al., 2017); an inference supported by bubble-reconstructed melt inclusions that have CO_2/ITE ratios in broad agreement with those of depleted inclusions (Fig. 4 & 5). Therefore, relative carbon enrichment in Miðfell was likely not restricted to the most ITE-depleted melts, but rather a characteristic of all ITE concentrations (Fig. 4a & 5). With this result, the key question is what source or process led to high CO_2/ITE ratios in Miðfell inclusions?

5.2. Crustal melt modification

Gurenko and Sobolev (2006) analysed olivine-hosted melt inclusions and gabbroic xenoliths from Miðfell to infer that the trace element chemistry of Miðfell melt inclusions had been modified by interaction with lower crustal gabbro. To attribute a carbon enrichment signature to the mantle, we must identify melt inclusions that have avoided CO_2/ITE ratio modification by crustal interaction.

We have modelled the mixing of a depleted Miðfell melt composition, which has a smooth trace element pattern, with crustal components. We discount a role for significant plagioclase addition to Miðfell melts (Fig. S5). However,

mixing with a 10% fractional melt derived from Miðfell gabbro best matches the shape of positive Sr, negative Zr, and Ba > Nb anomalies observed within some of the Miðfell melt inclusion population (Fig. 3 & S6), providing good evidence for interaction between primitive Miðfell melts and gabbro in the crust.

Extending our analysis to assess the impact of crustal interaction on CO_2/ITE ratios; an important observation is that carbonate phases have not been seen in Miðfell gabbroic xenoliths (Gurenko and Sobolev, 2006), though carbonate breakdown on decompression during eruption may remove visible evidence of gabbroic carbon (e.g., Canil, 1990). Therefore, the addition of carbon to Miðfell melts cannot be ruled out from textural observations, but geochemical observations can be used to avoid melt inclusions that have strongly interacted with gabbroic material, i.e., those having large trace element anomalies.

To avoid the effects of any potential CO_2-ITE modification, in the subsequent analysis we have only used melt inclusions with smooth trace element patterns. We believe that these melt inclusions have had minimal interaction with crustal gabbro during ascent through the Miðfell magmatic system.

Melt inclusions with smooth trace element patterns record maximum CO_2/Nb = 1832 ± 316 and CO_2/Ba = 396 ± 48 (Fig. 5c,d), again showing higher ratios than observed in MORB suites, and suggesting that the relative carbon enrichment in Miðfell melts likely originates in its source mantle.

6. Estimating the carbon content of the Miðfell mantle source

The key question we address in this section is whether the observed high CO_2/Ba and CO_2/Nb ratios in Miðfell inclusions require an anomalously carbon-rich mantle source. First we identify which ITE's have stayed coupled to carbon during the melting process, and hence which CO_2/ITE ratios are unfractionated from their source values. We then review the mantle components contributing

to Miðfell and calculate in what relative proportions they are represented in its chemistry. Finally, we use constraints on ITE concentrations in these sources to convert the observed CO_2 and ITE systematics of Miðfell inclusions into source CO_2 concentrations.

6.1. Carbon-ITE coupling in Miðfell

The silicate-melt partition coefficient for carbon, as estimated by carbonated-lherzolite melting experiments, places it between Ba and Nb in terms of compatibility (Rosenthal et al., 2015). Therefore, we would expect CO_2/Ba and CO_2/Nb in Miðfell to be similar to that of its mantle source, provided it represents an aggregation of melts from across the melting region (e.g., Fig. 6 solid line). If instead, Miðfell was produced from high-degree melts from the shallow part of the melting region, a region already extensively depleted by prior melting, then even highly incompatible elements may have been fractionated from each other, so CO_2/Ba and CO_2/Nb may not be faithful to the source value (e.g., Fig. 6 dashed and dashed-dotted lines).

We have two tests for whether CO_2/ITE ratios have been fractionated during melting. The first uses the fact that carbon partitioning between silicate and melt lies between that of Ba and Nb (Rosenthal et al., 2015). Therefore, if Miðfell represents preferential sampling of high-degree shallow melts, we might expect to observe anomalously high CO_2/Ba. However, this observation would be associated with correspondingly low CO_2/Nb. Instead, Miðfell inclusions show correlated high CO_2/Nb and CO_2/Ba values (Fig. 6), indicating that no such fractionation has occurred.

Secondly, fractionation between trace elements during fractional melting will be manifest in the elements' relative variability (their standard deviation divided by their mean concentration). One prediction of fractional melting models is that trace element variability should increase with decreasing partition coeffi-

cient (red line, Fig. 7; Schiano et al., 1993). Figure 7 shows that in Miðfell inclusions, the most incompatible elements measured (Ba, K, Nb, La) have constant relative variability, which is consistent with a residual porosity during melting having damped the variability generated by low degree melting. As these low degree melts will have contained almost all the Ba, K, Nb, and La that was in the source, these elements will not have been fractionated from each other during the melting event that produced Miðfell. As carbon's partition coefficient lies within the range of Ba to La, we can infer from Fig. 7 that carbon will not have been fractionated from any elements across this range of partition coefficients. Therefore, the uncommonly high CO_2/Ba and CO_2/Nb ratios observed in undegassed Miðfell melts (Fig. 5) reflect the composition of their mantle sources.

6.2. Components in the Miðfell mantle source

Miðfell's depleted mantle component: the Borgarhraun eruption provides an on-Iceland sample of the local depleted mantle component in the plume (Thirlwall et al., 2004; Stracke et al., 2003), one that has been suggested to be ubiquitous in the Atlantic mantle (Hauri et al., 2018). Similarities in lithophile elements (Fig. 3), including Pb isotopes (Kokfelt et al., 2006; Halldórsson et al., 2016a), between Miðfell and Borgarhraun, suggest that DMM-like Borgarhraun source material is also present as a component within the Miðfell mantle source.

Is there a pyroxenitic component in Miðfell?: The variability in trace element enrichment and major element chemistry of primitive melts from across Iceland has been interpreted to reflect recycled pyroxenitic components in the Icelandic mantle (Sobolev et al., 2008; Peate et al., 2010; Shorttle and Maclennan, 2011). In the case of Miðfell though, trace element ratios (e.g., Nb/Zr $\sim$0.05), major elements (FeO $\sim$9.4 wt%), and Cl isotopes (Halldórsson et al., 2016a) suggest a minimal contribution from pyroxenite material to this eruption.

This is not to say that Miðfell has had no recycled contribution to its composition. It contains a typical DMM component, which has itself been argued to contain recycled signatures, both as a regional contamination of the upper mantle (Hauri et al., 2018) and as a global phenomenon (Andersen et al., 2015). However, as Borgarhraun does not show significant carbon enrichment with respect to MORB and significantly less relative carbon enrichment than Miðfell, there is no evidence that the Icelandic mantle has been enriched in carbon from pyroxenite addition.

Evidence for a deep mantle component: the Miðfell source incorporates material distinct from that of the MORB source, having a more solar- or carbonaceous chondrite-like composition that is often ascribed to an ancient primordial reservoir. This signal is most distinct in the heavy noble gas isotopes (e.g., Harrison et al., 1999; Trieloff and Kunz, 2005; Mukhopadhyay, 2012; Caracausi et al., 2016).

However, the heavy noble gases also indicate that the Miðfell source has had atmosphere recycled into it (e.g., Harrison et al., 1999). This conclusion is in general consistent with constraints from other isotopic systems, e.g., N and Os, which suggest that ancient ($>$ 1.5 Ga) recycled crust is present within the deep mantle component of the Icelandic mantle plume as crustal isotopic signatures are coupled with high-$^{3}He/^{4}He$ values (Brandon et al., 2007; Halldórsson et al., 2016b). Therefore, a deep mantle component could contain carbon of both primordial and recycled origins.

The above observations suggest that the Miðfell source mantle comprises a mixture of a depleted component (DM), akin to Borgarhraun source mantle, and a deep mantle component (Deep). Both the Deep and DM components within the Miðfell source can have plausible estimates made of their ITE content, which will be important for estimating source CO_2 concentrations. In subsequent mod-

elling we adopt the BSE composition given by McDonough and Sun (1995) for the Deep component, though we note that its ITE composition could be more enriched due to recycled material. As there are no constraints on the nature of this enrichment, we do not propagate this uncertainty, although we emphasise that by assuming a BSE source rather than BSE + recycled source, our source carbon estimates will be a lower bound. We assign the DM component the Borgarhraun source mantle ITE composition (Hauri et al., 2018). As the CO_2 of DM has been estimated, only Deep CO_2 and the DM:Deep proportions are unknowns in estimating source CO_2. Neither choice of source composition is critical to the results we subsequently obtain: similar source carbon concentrations are inferred if we take, for example, ITE abundances from Palme and O'Neill (2014) for the Deep estimate and Workman and Hart (2005) for the DM.

6.3. Proportions of depleted and deep components in the Miðfell mantle source

If Ba, K, Nb, La, and carbon have not been fractionated from each other during melting, then their proportions in Miðfell reflect the degree of melting, F; melt mixing; and melt transport: partial melting will have enriched these ITE's in the melt compared to their source concentrations. Using estimates of Ba, K, Nb, and La content of both DM and Deep components constituting the Miðfell source, we can calculate how much the melting process has enriched Miðfell compared to its mantle source, and thereby calculate the source carbon content. We define the enrichment factor for an element, i, as

$$E_i = \frac{C_i^l}{C_i^0}, \tag{1}$$

where C_i^l is the concentration of the element in the liquid (i.e., observed Miðfell) and C_i^0 is the concentration of the element in the source (DM and Deep taken from Hauri et al., 2018 and McDonough and Sun, 1995, respectively). For Ba,

K, Nb, and La we can calculate E_i directly, assuming a DM:Deep ratio. For carbon, we take the mean enrichment factor estimated from the lithophile trace elements, and use it in (1) with the observed carbon content of Miðfell inclusions to estimate C_C^0. The main question is what mass fraction of the Miðfell source is the Deep component? The enrichment factor contains information on this fraction: given that Ba, K, Nb, and La have not been fractionated during melting, and if we have identified the correct Deep and DM source compositions, then $E_{\mathrm{Ba}} = E_{\mathrm{K}} = E_{\mathrm{Nb}} = E_{\mathrm{La}}$. Therefore, by sweeping through Deep component fractions from 0 to 1 and identifying the minimum amount of variability in E_i, we can identify the optimal source mixture.

In Fig. 8a we show the mean enrichment factor, $\bar{E}$, calculated from Ba, K, Nb, and La content of the Miðfell matrix glass (i.e., the composition of the aggregated melt) as a function of Deep fraction in the source. Figure 8 shows that $\bar{E}$ lies between 1 and 3 in these models. These small enrichment factors likely reflect both the high peak mantle melt extent under Iceland (∼30%; Maclennan et al., 2001) and the incomplete mixing of mantle melts leading to a bias towards relatively shallow fractional melts from the full melting column in the mean Miðfell composition.

When the source is mostly DM (i.e., low $\mathrm{X_{Deep}}$) the C_i^0 values are low, and the E_i's are correspondingly high. The variability in the calculated enrichment factors is minimised at $\mathrm{X_{Deep}} = 0.47$ (Fig. 8b), i.e., a nearly 50:50 mixture of DM and Deep components in the Miðfell source, which corresponds to $\bar{E} = 1.56$.

6.4. Translating enrichment factors to source CO_2

The final step in using the calculated enrichment factors to estimate bulk Miðfell source carbon is to choose a carbon content for the Miðfell magma. For this calculation we take the CO_2 content of the melt inclusions most chemically similar to the matrix glass, which have $\mathrm{CO_2} = 1079$ ppm: these inclusions likely

trap the mixed magma prior to its extensive low pressure degassing, albeit they do not have the highest CO_2/ITE ratios we observe and therefore may have already lost some CO_2. Most importantly, this choice is consistent with our use of the matrix glass trace element composition to calculate the enrichment factors. Our calculation is also independent of chosen DM CO_2 value, as it is determined by erupted CO_2 content and $\bar{E}$ values.

Taking this value of CO_2, Fig. 8c reports Miðfell source carbon content calculated using enrichment factors over a range of source Deep fractions (blue line). For $X_{Deep} = 0.47$, the bulk Miðfell source contains 690 ppm CO_2 (Fig. 8c green bar).

Mass balance between the DM and Deep components allows us to convert the bulk source CO_2 (blue) into Deep CO_2 (orange). Here our calculation does depend on knowing the DM CO_2 content, which has been previously constrained as 105 ± 57 ppm (black; Hauri et al., 2018). For $X_{Deep} = 0.47$, Deep has a CO_2 content of 1350 ± 350 ppm (90% confidence interval considering only propagated analytical and $\bar{E}$ uncertainties).

These calculations are robust for a number of different assumptions: (i) as Fig. 8c shows, the full range of source DM:Deep proportions predict a Deep CO_2 content > 1000 ppm; (ii) if the modelling is repeated using more depleted melt inclusions, which are less likely to have undergone degassing and have peak CO_2 of 300 ppm, then Deep compositions of > 1250 ppm CO_2 are inferred; and (iii) adaptations to the model to explore the consequences of mixing fractional melts from two sources produce the same requirement of > 1000 ppm CO_2 in the Deep source.

7. Summary & Discussion

We have shown that melt inclusions from the Icelandic Miðfell eruption record some of the highest CO_2/ITE ratios reported in basalts, and that these inclusions reflect the composition of their mantle source. In comparison with Borgarhraun, Miðfell's noble gas and lithophile element composition argues for its source comprising a deep mantle component in addition to the depleted mantle common to Icelandic magmas. By combining existing work with our new carbon and trace element observations, we have been able to assign a carbon content to this deep component. We took the depleted mantle component to be that of the well-studied Borgarhraun eruption, which lacks primitive noble gas isotope signatures and has a source $CO_2 = 105 \pm 57$ ppm (using Ba, Nb estimates; Hauri et al., 2018). We estimate the deep mantle component to have a CO_2 concentration of at least 1000 ppm (preferred value 1350 ± 350 ppm), which increases when the proportion of deep mantle component assumed to be present in the source is decreased.

7.1. Recycled carbon?

Xenon isotopes indicate that a significant proportion of Xe in Miðfell is derived from recycled air (∼90%; Mukhopadhyay, 2012). If carbon was coupled to Xe during recycling, then some amount of carbon in the Miðfell source could also have come from recycling. However, it would be surprising if this component was the origin of the high CO_2/ITE ratios we observe. Miðfell lavas are not unique in containing recycled air: MORB have been interpreted to have a similar abundance of recycled air in their DMM source (Mukhopadhyay, 2012; Parai and Mukhopadhyay, 2015). Moreover, DMM, in contrast to the Icelandic mantle, is also known from Pb isotopes, U isotopes, and CO_2/Ba ratios to have been pervasively contaminated by surface material (Andersen et al., 2015; Hirschmann, 2018). Despite this, MORB have lower CO_2/ITE and inferred

source CO_2 concentrations than Miðfell (e.g., Le Voyer et al., 2017). Therefore recycling, at least as seen by MORB, does not appear to significantly enrich carbon with respect to ITE's.

7.2. Ancient mantle carbon?

If Miðfell's carbon enrichment is a signature of entrained deep mantle material, to what extent is it ancient mantle carbon? This question is difficult to answer and will require more eruptions to be identified with primitive noble gas signatures and carbon undersaturated melt inclusions. However, the two eruptions we now have on Iceland with CO_2/ITE ratios that can be linked to their mantle sources, differ almost exclusively in their geochemistry by the presence of primitive noble gas signatures in Miðfell, which are absent in Borgarhraun — their lithophile radiogenic isotope compositions are otherwise very similar (Fig. 1b,c). This signature suggests an association between the primitive noble gases, which have been attributed to solar nebula ingassing during Earth's earliest history (Mukhopadhyay, 2012; Williams and Mukhopadhyay, 2018), and carbon. If true, it would imply a significant fraction of Earth's carbon came directly from the solar nebula rather than later accretion.

However, the coupling of high-$^3He/^4He$ with recycled material signatures (Brandon et al., 2007; Halldórsson et al., 2016b) could also suggest that deep mantle carbon is of a recycled origin, making it difficult to differentiate between primordial and recycled carbon from deep mantle material. Especially as there is no certainty that the nature of deep recycled material is the same as the upper mantle recycled material assumed to be present in the Borgarhraun source, which evidences no enrichment in carbon (Hauri et al., 2018).

7.3. Size of the PM carbon reservoir

If we assume that the Deep carbon estimate derived from Miðfell is representative of the global deep mantle reservoir, then we can calculate a revised

mantle carbon budget. Estimates for the deep mantle fraction of the total mantle range from the seismically-defined 660 km transition zone, down to the seismically-defined D" layer above the core-mantle boundary. Figure 9 presents carbon content estimates of four potential deep mantle reservoir fractions: (i) 5% representing the D" layer (blue; Tolstikhin and Hofmann, 2005); (ii) 20% for the abyssal layer of the lower mantle, defined by U/K mass balance (green; Arevalo et al., 2009); (iii) 42% for the mass of primitive mantle calculated by ^{40}Ar mass balance (orange; 90% confidence envelope in grey; this study and Allègre et al., 1996); and (iv) 75% for the lower mantle as defined by the 660 km seismic discontinuity (red; Hofmann, 1997).

The carbon content of the atmosphere, crust, and oceans combined (ACO) is $\sim 3.1 \times 10^{23}$ g CO_2 (Hirschmann, 2018). Carbon stored in the deep mantle, depending on mantle fraction, is therefore up to 14 times greater than the ACO carbon reservoir, while the DMM is approximately equal to the ACO (Fig. 9). Our calculations do not include the potential carbon contribution from the lithospheric mantle, which could be host to one AOC of carbon (Sleep, 2009; Kelemen and Manning, 2015). These carbon reservoir estimates for the deep Earth are necessarily speculative, but comparable to the range of previous bulk mantle estimates (e.g., Halliday, 2013). Our carbon estimates are also a lower bound in two important respects: (i) if the deep mantle component in Miðfell is less than the high value we used, then the implied carbon content in it is higher; (ii) if the deep component contains recycled material that is enriched in Ba and Nb, then our use of a BSE composition will have led to an underestimate of its carbon content.

Acknowledgements

Funding: This work is based on observations made using the Natural Environment Research Council (NERC) Edinburgh Ion microprobe facility under grant number IMF523/0514, and the STFC Diamond Light source facility under grant number SP11208. W.M. was funded by NERC studentship number NE/L501578/1. O.S. was funded by Trinity College Cambridge through a Title A Fellowship, and at Caltech by a Geology Option Postdoctoral Fellowship. G.G. was funded by National Science Foundation (NSF) grant number NSF OCE-1459649. Ion microprobe analyses at the Northeast National Ion Microprobe Facility at Woods Hole Oceanographic Institution were partially subsidized by the Instrumentation and Facilities Program, Division of Earth Sciences, NSF. **Competing interests:** The authors declare that they have no competing financial interests.

Tables

Setting	Ocean Island				Mid Ocean Ridge			
Locality	Miðfell		Borgarhraun	Hawaii	Eq. MAR	Siquieros	14°N MAR	Global MORB
Reference	This study		Hauri et al. (2018)	Anderson & Poland (2017)	Le Voyer et al. (2017)	Saal et al. (2002)	Cartigny et al. (2008)	Michael & Graham (2015)
	Bulk	Deep						
CO_2/Nb	1832	> 1520	391	758	557	230	534	607
CO_2/Ba	396	> 150	48.3	86	96.6	74.2	106	105
Mantle CO_2 (Nb)	887	-	129	-	48	23	393	90
Mantle CO_2 (Ba)	1580	-	80	-	22	24	427	59
Mantle CO_2 (other)	> 690	> 1000	-	263	-	-	-	-
Nb ppm	0.484	0.658	0.330	0.347	0.0862	0.100	0.736	0.149
Ba ppm	3.99	6.60	1.66	3.06	0.228	0.323	4.04	0.562

Table 1: Estimates of mantle carbon reservoirs. This study presents carbon estimates for Miðfell source mantle and a deep mantle reservoir, calculated from olivine-hosted melt inclusion compositions and a DM–Deep mixing model. CO_2/ITE ratios for each data set are as published in their original publications. Source trace element and CO_2 estimates are the values presented by Hauri et al. (2018), who used the method of Shimizu et al. (2016) to calculate source trace element concentrations.

Figures

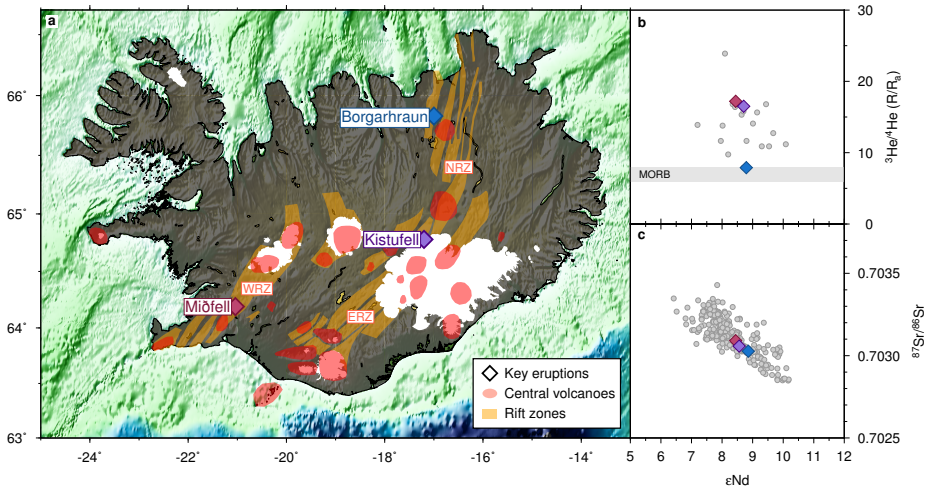

Figure 1: Icelandic eruptions discussed in this study: Miðfell (red), Kistufell (purple), and Borgarhraun (blue). Map of Iceland in (a) shows eruption locations, central volcanoes (red areas), and main rift zones (orange): WRZ, western rift zone; ERZ, eastern rift zone; and NRZ, northern rift zone. In (b) He isotope compositions relative to atmospheric ^{3}He/^{4}He (R/R$_a$) and in (c) Sr isotope compositions against ϵNd for key eruptions (diamonds) and young Icelandic eruptions ($<$ 120 kyrs) from rift zones (grey). Kistufell and Miðfell show elevated ^{3}He/^{4}He with respect to Borgarhraun. Data compiled in Shorttle and Maclennan (2011).

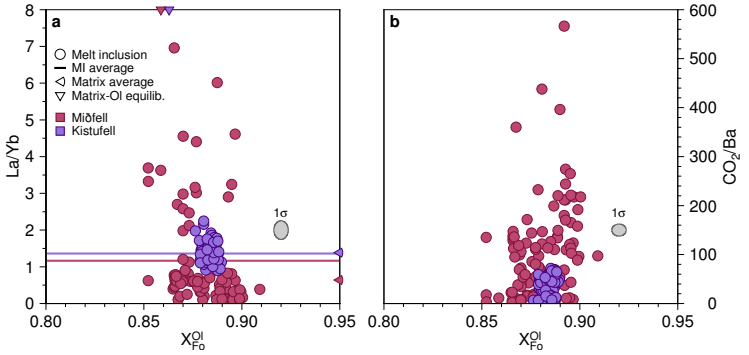

Figure 2: (a) La/Yb ratio of Miðfell (red) and Kistufell (purple) melt inclusions against host olivine forsterite content. Average melt inclusion La/Yb ratios are shown by horizontal lines, while matrix glass averages are indicated by arrowheads at $X_{Fo}^{Ol} = 0.95$. The olivine forsterite compositions in equilibrium with the matrix glasses are shown by inverted triangles at La/Yb = 8. Melt inclusion variability is preserved with decreasing forsterite content in the Miðfell suite, while the Kistufell melt inclusions have much lower La/Yb variability and are clustered within a smaller forsterite content range. (b) CO_2/Ba against forsterite, indicating that the highest CO_2/Ba ratios are preserved in the most forsteritic olivines. One sigma error ellipse plotted in grey.

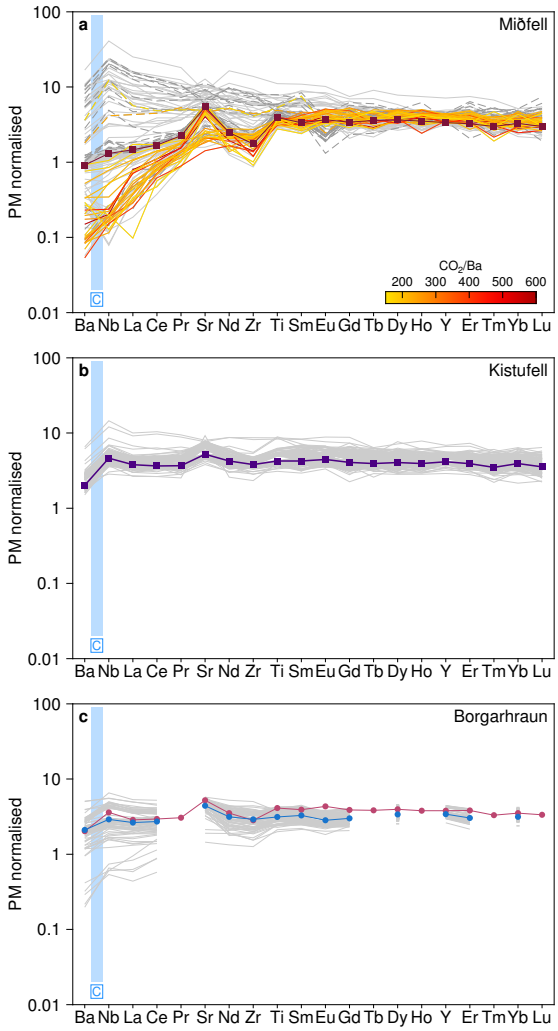

Figure 3: Trace element spider diagrams showing compositional variability in (a) Miðfell, (b) Kistufell, and (c) Borgarhraun (Hauri et al., 2018) melt inclusion suites, normalised to primitive mantle (PM; BSE composition, McDonough and Sun, 1995). Inclusions with $CO_2/Ba > 150$ are coloured, the rest are grey (Borgarhraun melt inclusions have an average $CO_2/Ba \sim 48$). Matrix glass compositions are shown as dark squares. The likely position of carbon, given its measured compatibility (Rosenthal et al., 2015), is shown as a blue vertical line. In (c) the light red line and circles are the Miðfell average melt inclusion composition, and in light blue is the Borgarhraun melt inclusion average. Miðfell and Borgarhraun matrix glasses are very similar, but Miðfell shows greater trace element variability within the melt inclusion population.

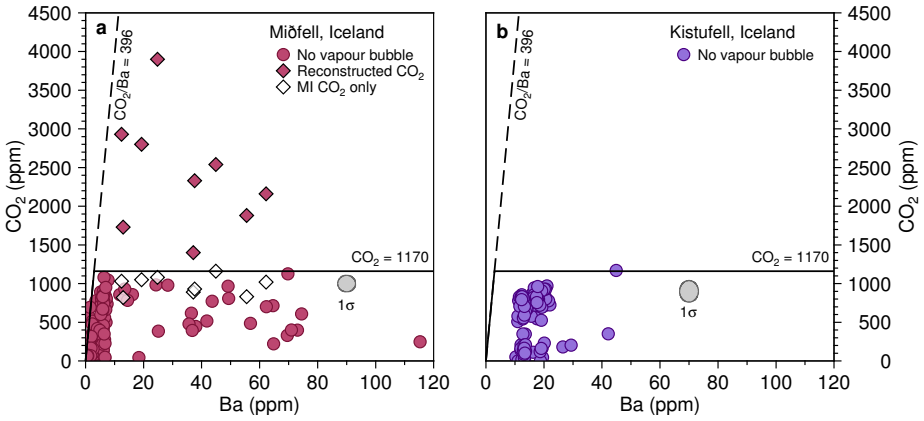

Figure 4: Variation in CO_2 content as a function of Ba concentration for (a) Miðfell and (b) Kistufell melt inclusions (diamonds, with vapour bubbles; circles, without vapour bubbles). The maximum CO_2 recovered from melt inclusion glass (circles and unfilled diamonds) is 1170 ppm, as shown by the horizontal line. Combined glass and vapour bubble CO_2 measurements plot between this line and $CO_2/Ba = 396$ (the maximum ratio preserved by a smooth trace element pattern melt inclusion), as shown by the dashed line. Miðfell contains melt inclusions with low enough Ba concentrations that they have likely avoided degassing, while Kistufell melt inclusions are too enriched and have all likely lost CO_2. One sigma error ellipse plotted in grey.

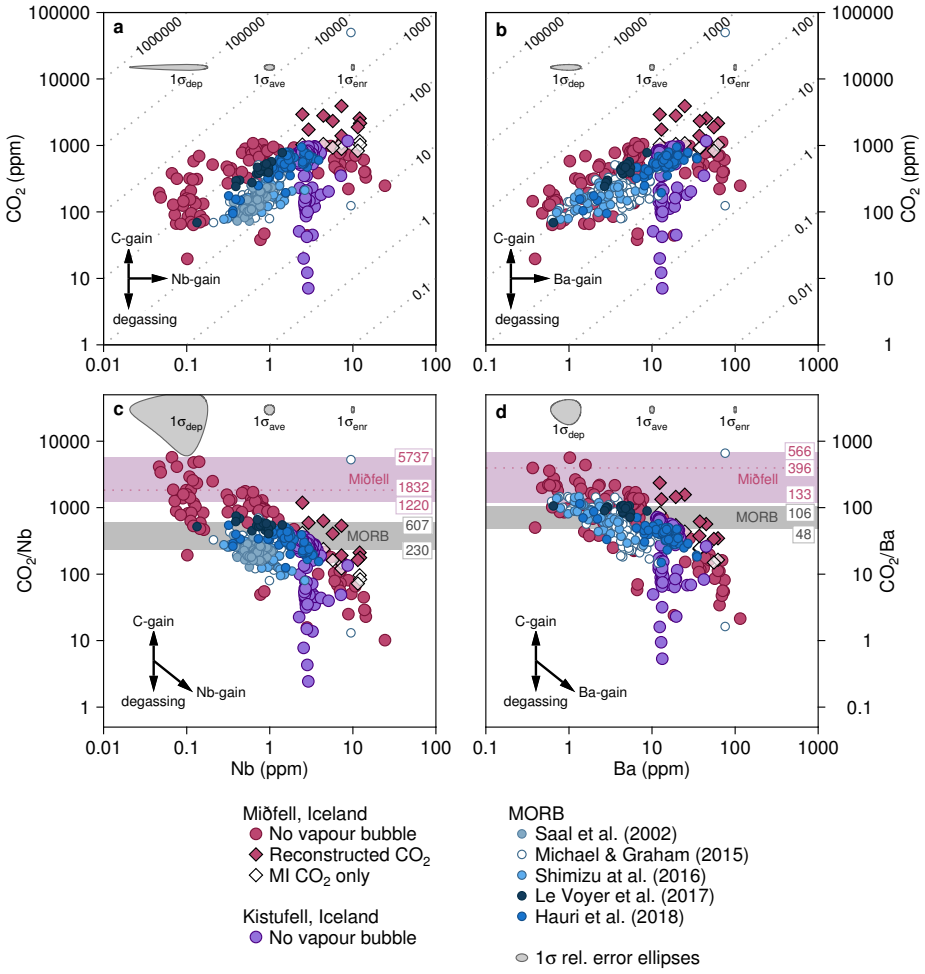

Figure 5: CO_2 content against (a) Nb abundance and (b) Ba abundance, and CO_2/ITE against ITE for (c) Nb and (d) Ba, for melt inclusion and glass suites. Miðfell melt inclusions (red) were measured at Edinburgh (circles) and Woods Hole Oceanic Institution (diamonds). Filled diamonds show reconstructed CO_2 content, while empty diamonds are glass only CO_2. Previously analysed suites are from Siquieros (light blue; Saal et al., 2002), Borgarhraun (royal blue; Hauri et al., 2018), and Equatorial Atlantic (dark blue; Le Voyer et al., 2017) melt inclusions, and MORB glasses (white, Michael and Graham, 2015; sky blue, D-MORB, Shimizu et al., 2016). Dashed lines show constant CO_2/ITE ratios in (a) & (b). Light red regions in (c) & (d) indicate the maximum CO_2/ITE ratios recorded (from high to low) in: (i) the whole population, (ii) melt inclusions with a smooth trace element pattern, and (iii) melt inclusions with matrix glass ITE concentration. Miðfell contains melt inclusions that are enriched in carbon with respect to MORB suites and Kistufell for a range of ITE concentrations. Grey bands show MORB source estimates. One sigma error ellipses are dependent on trace element concentration.

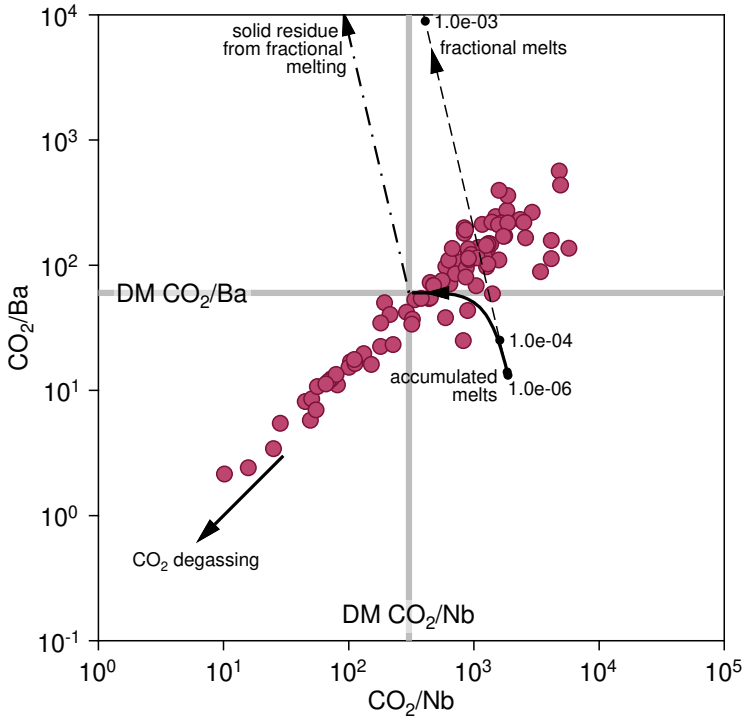

Figure 6: The relationship between CO_2/Nb and CO_2/Ba in Miðfell melt inclusions. The CO_2/ITE ratios of the depleted mantle component (DM), as inferred from the Borgarhraun eruption, are shown as grey bars. These ratios represent the starting source composition for modelling fractional melting. The composition of instantaneous melts of this source follow the dashed line, accumulated melts the solid line, and the residual solid the dashed-dotted line. Points along the instantaneous melts curve are labelled by melt fraction. The highest CO_2/ITE melts cannot be produced by fractional melting of a DM source. Partition coefficients for melting were taken from Rosenthal et al. (2015): $D_{\mathrm{C}} = 0.00055$, $D_{\mathrm{Nb}} = 0.0034$, and $D_{\mathrm{Ba}} = 0.00012$.

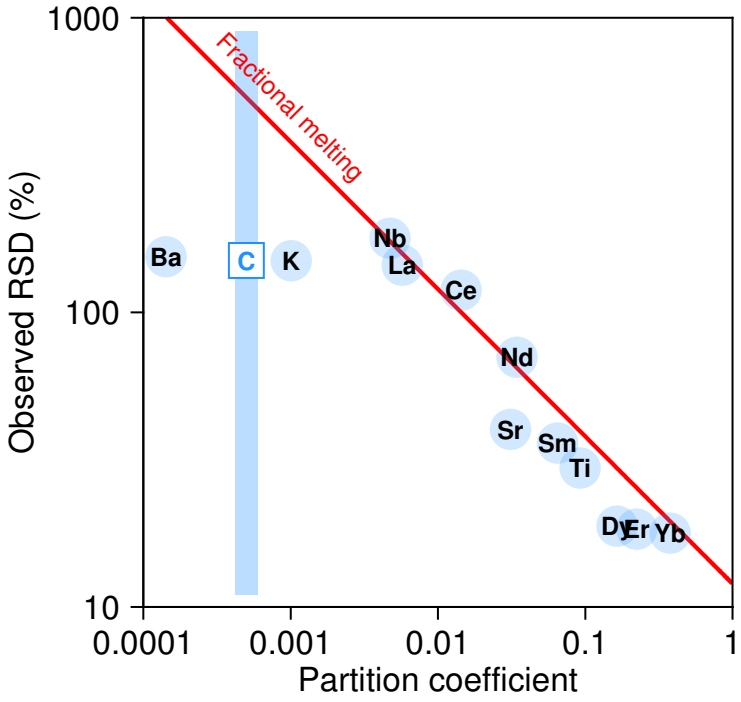

Figure 7: Trace element variability in Miðfell melt inclusions shown by observed relative standard deviation (RSD) of trace elements with varying incompatibility on mantle melting. The results of a pure fractional melting model and the partition coefficients for garnet peridotite melting are shown as a red solid line. The expected behaviour of carbon can be inferred from the blue vertical line, based on its measured compatibility (Rosenthal et al., 2015). Ba, K, Nb, La show similar RSD, suggesting that they remained coupled during melting.

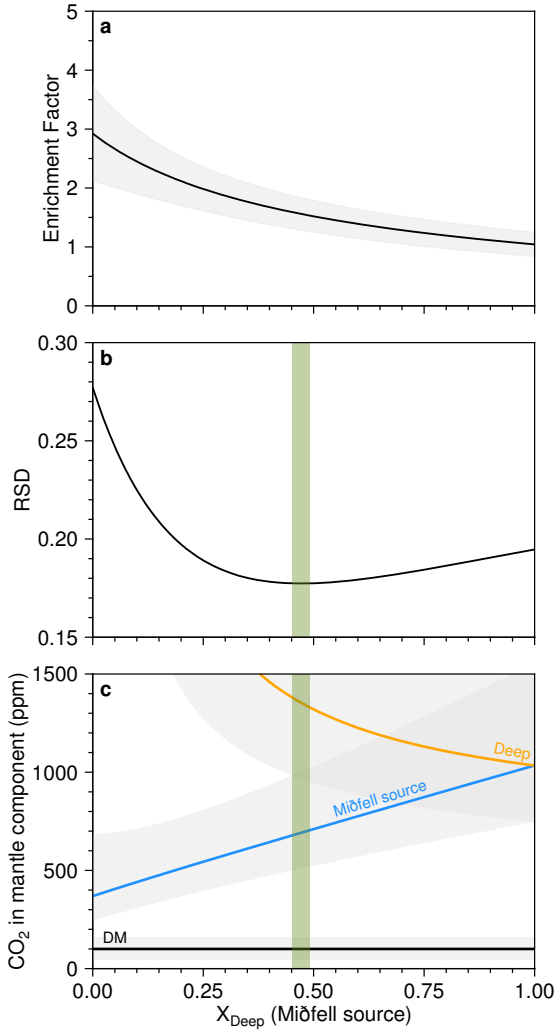

Figure 8: Estimating the fraction of deep mantle component (X_{Deep}) in the Miðfell source (a & b), and the CO_2 concentration of the bulk Miðfell source and its depleted (DM) and deep (Deep) components (c). The best-fit mean enrichment factor ($\bar{E}$) calculated from Ba, K, Nb and La in Miðfell relative to a mixed source (a; 2σ error as grey field) is defined by the X_{Deep} composition where relative standard deviation of the enrichment factor for the four elements is minimised (b; green band). In (c), the Miðfell source CO_2 content was calculated using $\bar{E}$ and measured CO_2 (= 1079 ppm). The CO_2 concentration of the Deep component (orange) was calculated by balancing the Miðfell source content with the DM component (105 $\pm$ 57 ppm; black; Ba and Nb estimate average from Hauri et al., 2018). 90% confidence envelopes in grey.

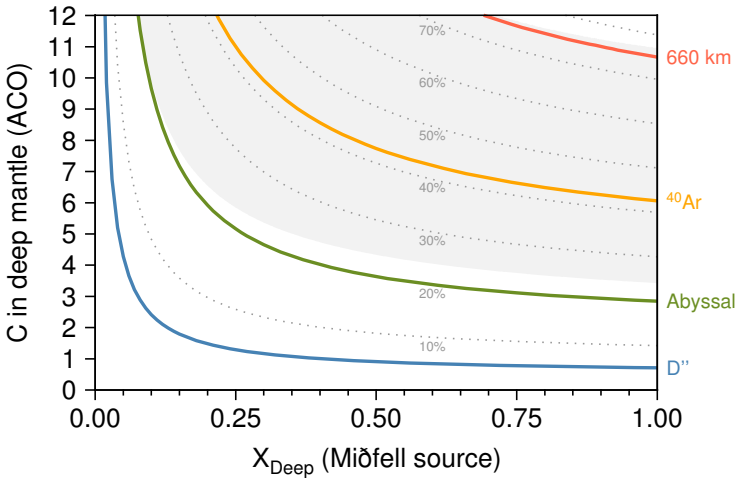

Figure 9: Estimates of deep mantle carbon reservoir mass (ACO = Atmosphere + Crust + Oceans = 3.1×10^{23} g CO_2), using the Deep concentration curve in Fig. 8c for a range of mantle fractions (grey dotted lines). Four mantle fractions have been highlighted: (i) 5% representing the seismically-defined D" layer (blue; Tolstikhin and Hofmann, 2005); (ii) 20% for the abyssal layer of the lower mantle, defined by U/K mass balance (green; Arevalo et al., 2009); (iii) 42% for the mass of primitive mantle calculated by ^{40}Ar mass balance (orange; 90% confidence envelope in grey; this study and Allègre et al., 1996); and (iv) 75% for the lower mantle as defined by the 660 km seismic discontinuity (red; Hofmann, 1997).

References

Allègre, C.J., Hofmann, A., O'Nions, K., 1996. The argon constraints on mantle structure. Geophysical Research Letters 23, 3555–3557.

Andersen, M.B., Elliott, T., Freymuth, H., Sims, K.W.W., Niu, Y., Kelley, K.A., 2015. The terrestrial uranium isotope cycle. Nature 517, 356–359.

Anderson, K.R., Poland, M.P., 2017. Abundant carbon in the mantle beneath Hawai'i. Nature Geoscience 10, 704–708.

Arevalo, R., McDonough, W.F., Luong, M., 2009. The K/U ratio of the silicate Earth: Insights into mantle composition, structure and thermal evolution. Earth and Planetary Science Letters 278, 361–369. doi:10.1016/j.epsl.2008.12.023.

Brandon, A.D., Graham, D.W., Waight, T., Gautason, B., 2007. ^{186}Os and ^{187}Os enrichments and high ^{3}He/^{4}He sources in the Earth's mantle: Evidence from Icelandic picrites. Geochimica et Cosmochimica Acta 71, 4570–4591.

Breddam, K., 2002. Kistufell: Primitive melt from the Iceland mantle plume. Journal of Petrology 43, 345–373.

Breddam, K., Kurz, M.D., Storey, M., 2000. Mapping out the conduit of the Iceland mantle plume with helium isotopes. Earth and Planetary Science Letters 176, 45–55.

Canil, D., 1990. Experimental study bearing on the absence of carbonate in mantle-derived xenoliths. Geology 18, 1011–1013.

Caracausi, A., Avice, G., Burnard, P.G., Füri, E., Marty, B., 2016. Chondritic xenon in the Earth's mantle. Nature 533, 82–85. doi:10.1038/nature17434.

663 Cartigny, P., Pineau, F., Aubaud, C., Javoy, M., 2008. Towards a consistent
664 mantle carbon flux estimate: Insights from volatile systematics (H_2O/Ce,
665 δD, CO_2/Nb) in the North Atlantic mantle (14° N and 34° N). Earth and
666 Planetary Science Letters 265, 672–685.

667 Danyushevsky, L.V., Della-Pasqua, F.N., Sokolov, S., 2000. Re-equilibration of
668 melt inclusions trapped by magnesian olivine phenocrysts from subduction-
669 related magmas: petrological implications. Contributions to Mineralogy and
670 Petrology 138, 68–83. doi:10.1007/PL00007664.

671 Dasgupta, R., Hirschmann, M.M., 2010. The deep carbon cycle and melting in
672 Earth's interior. Earth and Planetary Science Letters 298, 1–13.

673 Füri, E., Hilton, D.R., Halldórsson, S.A., Barry, P.H., Hahm, D., Fischer, T.P.,
674 Grönvold, K., 2010. Apparent decoupling of the He and Ne isotope systematics
675 of the Icelandic mantle: The role of He depletion, melt mixing, degassing
676 fractionation and air interaction. Geochimica et Cosmochimica Acta 74, 3307–
677 3332.

678 Gonnermann, H.M., Mukhopadhyay, S., 2007. Non-equilibrium degassing and
679 a primordial source for helium in ocean-island volcanism. Nature 449, 1037–
680 1040. doi:10.1038/nature06240.

681 Gurenko, A.A., Chaussidon, M., 1995. Enriched and primitive melts included
682 in olivine from Icelandic tholeiites: origin by continuous melting of a single
683 mantle column. Geochimica et Cosmochimica Acta 59, 2905–2917.

684 Gurenko, A.A., Sobolev, A.V., 2006. Crust-primitive magma interaction be-
685 neath neovolcanic rift zone of Iceland recorded in gabbro xenoliths from Mid-
686 fell, SW Iceland. Contributions to Mineralogy and Petrology 151, 495–520.

687 Halldórsson, S.A., Barnes, J.D., Stefánsson, A., Hilton, D.R., Hauri, E.H., Mar-
688 shall, E.W., 2016a. Subducted lithosphere controls halogen enrichments in
689 the Iceland mantle plume source. Geology 44, 679–682.

690 Halldórsson, S.A., Hilton, D.R., Barry, P.H., Füri, E., Grönvold, K., 2016b.
691 Recycling of crustal material by the Iceland mantle plume: New evidence from
692 nitrogen elemental and isotope systematics of subglacial basalts. Geochimica
693 et Cosmochimica Acta 176, 206–226. doi:10.1016/j.gca.2015.12.021.

694 Halliday, A.N., 2013. The origins of volatiles in the terrestrial planets. Geochim-
695 ica et Cosmochimica Acta 105, 146–171.

696 Harrison, D., Burnard, P., Turner, G., 1999. Noble gas behaviour and composi-
697 tion in the mantle: constraints from the Iceland Plume. Earth and Planetary
698 Science Letters 171, 199–207.

699 Hartley, M.E., Neave, D.A., Maclennan, J., Edmonds, M., Thordarson, T.,
700 2015. Diffusive over-hydration of olivine-hosted melt inclusions. Earth and
701 Planetary Science Letters 425, 168–178.

702 Hauri, E.H., Maclennan, J., McKenzie, D., Gronvold, K., Oskarsson, N.,
703 Shimizu, N., 2018. CO_2 content beneath northern Iceland and the variability
704 of mantle carbon. Geology 46, 55–58.

705 Hayes, J.M., Waldbauer, J.R., 2006. The carbon cycle and associated redox
706 processes through time. Philosophical Transactions of the Royal Society B
707 361, 931–950.

708 Hirschmann, M.M., 2016. Constraints on the early delivery and fractionation
709 of Earth's major volatiles from C/H, C/N, and C/S ratios. American Miner-
710 alogist 101, 540–553.

Hirschmann, M.M., 2018. Comparative deep Earth volatile cycles: The case for C recycling from exosphere/mantle fractionation of major (H_2O, C, N) volatiles and from H_2O/Ce, CO_2/Ba, and CO_2/Nb exosphere ratios. Earth and Planetary Science Letters 502, 262–273. doi:10.1016/j.epsl.2018.08.023.

Hofmann, A.W., 1997. Mantle geochemistry: the message from oceanic volcanism. Nature 385, 219–229.

Jenkins, J., Cottaar, S., White, R.S., Deuss, A., 2016. Depressed mantle discontinuities beneath Iceland: Evidence of a garnet controlled 660 km discontinuity? Earth and Planetary Science Letters 433, 159–168.

Kelemen, P.B., Manning, C.E., 2015. Reevaluating carbon fluxes in subduction zones, what goes down, mostly comes up. Proceedings of the National Academy of Sciences 112, E3997–E4006. doi:10.1073/pnas.1507889112.

Kokfelt, T., Hoernle, K., Hauff, F., Fiebig, J., Werner, R., Garbe-Schönberg, D., 2006. Combined trace element and Pb-Nd-Sr-O isotope evidence for recycled oceanic crust (upper and lower) in the Iceland mantle plume. Journal of Petrology 47, 1705–1749.

Le Voyer, M., Kelley, K., Cottrell, E., Hauri, E., 2017. Heterogeneity in mantle carbon content from CO_2-undersaturated basalts. Nature Communications 8, 14062.

Maclennan, J., 2008a. Concurrent mixing and cooling of melts under Iceland. Journal of Petrology 49, 1931–1953. doi:10.1093/petrology/egn052.

Maclennan, J., 2008b. Lead isotope variability in olivine-hosted melt inclusions from Iceland. Geochimica et Cosmochimica Acta 72, 4159–4176.

735 Maclennan, J., 2017. Bubble formation and decrepitation control the CO_2 con-
736 tent of olivine-hosted melt inclusions. Geochemistry, Geophysics, Geosystems
737 18, 597–616. doi:10.1002/2016GC006633.

738 Maclennan, J., McKenzie, D., Grönvold, K., 2001. Plume-driven upwelling
739 under central Iceland. Earth and Planetary Science Letters 194, 67–82.

740 Maclennan, J., McKenzie, D., Hilton, F., Gronvöld, K., Shimizu, N., 2003.
741 Geochemical variability in a single flow from northern Iceland. Journal of
742 Geophysical Research 108. doi:10.1029/2000JB000142.

743 Marty, B., 2012. The origins and concentrations of water, carbon, nitrogen and
744 noble gases on Earth. Earth and Planetary Science Letters 313-314, 56–66.

745 Matthews, S., Shorttle, O., Rudge, J.F., Maclennan, J., 2017. Constraining
746 mantle carbon: CO_2-trace element systematics in basalts and the roles of
747 magma mixing and degassing. Earth and Planetary Science Letters 480, 1–
748 14. doi:10.1016/j.epsl.2017.09.047.

749 Matzen, A.K., Baker, M.B., Beckett, J.R., Stolper, E.M., 2011. Fe-Mg parti-
750 tioning between olivine and high-magnesian melts and the nature of Hawai-
751 ian parental liquids. Journal of Petrology 52, 1243–1263. doi:10.1093/
752 petrology/egq089.

753 McDonough, W.F., Sun, S., 1995. The composition of the Earth. Chemical
754 Geology 120, 223–253.

755 Michael, P.J., Graham, D.W., 2015. The behavior and concentration of CO_2
756 in the suboceanic mantle: Inferences from undegassed ocean ridge and ocean
757 island basalts. Lithos 236-237, 338–351.

758 Mojzsis, S.J., Harrison, T.M., Pidgeon, R.T., 2001. Oxygen-isotope evidence

759 from ancient zircons for liquid water at the Earth's surface 4,300 Myr ago.
760 Nature 409, 178–181.

761 Montelli, R., Nolet, G., Dahlen, F.A., Masters, G., 2006. A catalogue of deep
762 mantle plumes: New results from finite-frequency tomography. Geochemistry,
763 Geophysics, Geosystems 7. doi:10.1029/2006GC001248.

764 Mukhopadhyay, S., 2012. Early differentiation and volatile accretion recorded
765 in deep-mantle neon and xenon. Nature 486, 101–104.

766 Nestola, F., Korolev, N., Koylova, M., Rotiroti, N., Pearson, D.G., Pamato,
767 M.G., Alvaro, M., Peruzzo, L., Gurney, J.J., Moore, A.E., Davidson, J.,
768 2018. $CaSiO_3$ perovskite in diamond indicates the recycling of oceanic crust
769 into the lower mantle. Nature 555, 237–241. doi:10.1038/nature25972.

770 Palme, H., O'Neill, H., 2014. Cosmochemical Estimates of Mantle Composition,
771 in: Treatise on Geochemistry. 2 ed.. Elsevier. volume 3, pp. 1–39. doi:10.
772 1016/B978-0-08-095975-7.00201-1.

773 Parai, R., Mukhopadhyay, S., 2015. The evolution of MORB and plume mantle
774 volatile budgets: Constraints from fission Xe isotopes in Southwest Indian
775 Ridge basalts. Geochemistry, Geophysics, Geosystems 16, 719–735. doi:10.
776 1002/2014GC005566.

777 Peate, D.W., Breddam, K., Baker, J.A., Kurz, M.D., Barker, A.K., Prestvik,
778 T., Grassineau, N., Skovgaard, A.C., 2010. Compositional characteristics
779 and spatial distribution of enriched Icelandic mantle components. Journal of
780 Petrology 51, 1447–1475. doi:10.1093/petrology/egq025.

781 Peters, B.J., Carlson, R.W., Day, J.M.D., Horan, M.F., 2018. Hadean silicate
782 differentiation preserved by anomalous $^{142}Nd/^{144}Nd$ ratios in the Réunion
783 hotspot source. Nature 555. doi:10.1038/nature25754.

784 Rosenthal, A., Hauri, E., Hirschmann, M., 2015. Experimental determination
785 of C, F, and H partitioning between mantle minerals and carbonated basalt,
786 CO_2/Ba and CO_2/Nb systematics of partial melting, and the CO_2 contents
787 of basaltic source regions. Earth and Planetary Science Letters 412, 77–87.

788 Saal, A.E., Hauri, E., Langmuir, C.H., Perfit, M., 2002. Vapour undersaturation
789 in primitive mid-ocean-ridge basalt and the volatile content of Earth's upper
790 mantle. Nature 419, 451–455.

791 Schiano, P., Allègre, C.J., Dupré, B., Lewin, E., Joron, J.L., 1993. Variability
792 of trace elements in basaltic suites. Earth and Planetary Science Letters 119,
793 37–51.

794 Shimizu, K., Saal, A.E., Myers, C.E., Nagle, A.N., Hauri, E.H., Forsyth, D.W.,
795 Kamenetsky, V.S., Niu, Y., 2016. Two-component mantle melting-mixing
796 model for the generation of mid-ocean ridge basalts: Implications for the
797 volatile content of the Pacific upper mantle. Geochimica et Cosmochimica
798 Acta 176, 44–80.

799 Shishkina, T., Botcharnikov, R., Holtz, F., Almeev, R., Portnyagin, M., 2010.
800 Solubility of H_2O- and CO_2-bearing fluids in tholeiitic basalts at pressures up
801 to 500 MPa. Chemical Geology 277, 115–125.

802 Shorttle, O., 2015. Geochemical variability in MORB controlled by concurrent
803 mixing and crystallisation. Earth and Planetary Science Letters 424, 1–14.

804 Shorttle, O., Maclennan, J., 2011. Compositional trends of Icelandic basalts:
805 Implications for short-lengthscale lithological heterogeneity in mantle plumes.
806 Geochemistry, Geophysics, Geosystems 12. doi:10.1029/2011GC003748.

807 Shorttle, O., Maclennan, J., Piotrowski, A.M., 2013. Geochemical provincialism
808 in the Iceland plume. Geochimica et Cosmochimica Acta 122, 363–397.

809 Sleep, N.H., 2009. Stagnant lid convection and carbonate metasomatism of
810 the deep continental lithosphere. Geochemistry, Geophysics, Geosystems 10.
811 doi:10.1029/2009GC002702.

812 Sobolev, A.V., Hofmann, A.W., Brügmann, G., Batanova, V.G., Kuzmin, D.V.,
813 2008. A quantitative link between recycling and osmium isotopes. Science
814 321, 321.

815 Sobolev, A.V., Hofmann, A.W., Sobolev, S.V., Nikogosian, I.K., 2005. An
816 olivine-free mantle source of Hawaiian shield basalts. Nature 434, 412–417.

817 Stracke, A., 2012. Earth's heterogeneous mantle: a product of convection driven
818 interaction between crust and mantle. Chemical Geology 330–331, 274–299.

819 Stracke, A., Zindler, A., Salters, V.J.M., McKenzie, D., Blichert-Toft, J., Al-
820 barède, F., Grönvold, K., 2003. Theistareykir revisited. Geochemistry, Geo-
821 physics, Geosystems 4. doi:10.1029/2001GC000201.

822 Thirlwall, M.F., Gee, M.A.M., Taylor, R.N., Murton, B.J., 2004. Mantle com-
823 ponents in Iceland and adjacent ridges investigated using double-spike Pb
824 isotope ratios. Geochimica et Cosmochimica Acta 68, 361–386.

825 Tolstikhin, I., Hofmann, A.W., 2005. Early crust on top of the Earth's core.
826 Physics of the Earth and Planetary Interiors 148, 109–130. doi:10.1016/j.
827 pepi.2004.05.011.

828 Trieloff, M., Kunz, J., 2005. Isotope systematics of noble gases in the Earth's
829 mantle: possible sources of primordial isotopes and implications for mantle
830 structure. Physics of the Earth and Planetary Interiors 148, 13–38.

831 Trieloff, M., Kunz, J., Clague, D.A., Harrison, D., Allègre, C.J., 2000. The
832 nature of pristine noble gases in mantle plumes. Science 288, 1036–1038.

Walker, J.C.G., Hayes, P.B., Kasting, J.F., 1981. A negative feedback mechanism for the long-term stabilization of Earth's surface temperature. Journal of Geophysical Research 86, 9776–9782.

Williams, C.D., Mukhopadhyay, S., 2018. Capture of nebular gases during Earth's accretion is preserved in deep-mantle neon. Nature doi:10.1038/s41586-018-0771-1.

Workman, R.K., Hart, S.R., 2005. Major and trace element composition of the depleted MORB mantle (DMM). Earth and Planetary Science Letters 231, 53–72. doi:10.1016/j.epsl.2004.12.005.

Yuan, K., Romanowicz, B., 2017. Seismic evidence for partial melting at the root of major hot spot plumes. Science 357, 393–397.